DOI:10.7598/cst2017.1300 Chemical Science Transactions
ISSN:2278-3458 2017, **6(1),** 13-26

RESEARCH ARTICLE

Structural, Morphological, Magnetic and Impedance Studies of Layered $LiNi_{1/3}Co_{1/3}Mn_{1/3}O_2$ Cathode Material for Lithium Ion Batteries

G. TEWODROS AREGAI[1], K.VIJAYA BABU[2*], B.VIKRAM BABU[1], N.MURALI[2], K.EPHRAIM BABU[1], P.S.V. SUBBA RAO[1] and V.VEERAIAH[1]

[1]Department of Physics, Andhra University, Visakhapatnam, India
[2]Advanced Analytical Laboratory, Andhra University, Visakhapatnam, India
vijayababu.k@gmail.com

Received 19 July 2016 / Accepted 14 August 2016

Abstract: $LiNi_{1/3}Co_{1/3}Mn_{1/3}O_2$ was synthesized by solid state reaction method and the effect of calcination temperature on characteristics of $LiNi_{1/3}Co_{1/3}Mn_{1/3}O_2$ cathode was investigated. Thermal analysis reveals the temperature dependence of the materials properties. The phase composition, micro-morphology, elemental analysis and Wyckoff sites of the products were characterized by x-ray diffraction (XRD), scanning electron microscopy (SEM), energy dispersive spectra (EDS) and Fourier transform infrared (FTIR) respectively. The results of XRD pattern possessed the α-$NaFeO_2$ structure of the hexagonal system (space group $R\,\bar{3}\,m$). The morphological features of the powders were characterized by scanning electron microscopy (SEM). The EDS spectra confirm the presence of Ni, Co, Mn and O in the compound. The FT-IR spectroscopic data reveals that the structure of the oxide lattice constituted by LiO_6, NiO_6, CoO_6 and MnO_6 octahedral. The variation of the ac conductivity, dielectric constant and electric modulus as function of frequency and temperature was determined to study the electrical properties of the synthesized sample. Electron spin resonance (ESR) was carried out to study the magnetic properties as well. From this study, we conclude that the layered $LiNi_{1/3}Co_{1/3}Mn_{1/3}O_2$ material prepared by solid-state reaction method at 900 °C for 18h is promising next-generation cathode material for lithium ion batteries.

Keywords: Layered structure, Lithium nickel manganese cobalt oxides, XRD, SEM

Introduction

Over the past years of lithium-ion battery research, layered alkali transition metal oxide such as $LiCoO_2$ has stimulated substantial interests owing to its stability and high rate capability[1,2]. The need to enhance the performance of layered $LiCoO_2$, $LiMnO_2$ and $LiNiO_2$ cathode materials has logically lead to the intention of the mixed transition metal oxides as the alternative cathode materials. Lithium cobalt nickel manganese oxides $LiCo_xMn_yNi_{1-x-y}O_2$ were proposed as possible candidates to replace $LiCoO_2$ cathode[3,4]. This material adopts rhombohedra structure of $LiCoO_2$ and $LiNiO_2$. The composition of $LiCo_{1/3}Ni_{1/3}Mn_{1/3}O_2$,

referred in the literature as the 333 material[5], contains equal amounts of the transition metals Co, Mn, and Ni; it has high capacity[6] and good rate capability[7]. Taking away the lithium from the cathode materials leads to the structural changes followed by the cell volume change. This volume change could cause the mechanical rupture upon cycling. It was reported that the change in the cell volume for the 333 material $LiCo_xMn_yNi_{1-x-y}O_2$ is about 2%, which is much less than[8] 5% for $LiCo_xNi_{1-x}O_2$. This small volume change is associated with compensating changes in a and *c* parameters, that is, when the *c* parameter increases, the *a* parameter contracts and vice versa. This may play an important role in the cycle performance improvement of the cathode material. Along with the advantages mentioned above, in its oxidized state $LiCo_{1/3}Ni_{1/3}Mn_{1/3}O_2$ is less oxidative toward the electrolyte[9] than $LiCoO_2$ or $LiNiO_2$. This material has better thermal stability than $LiNiO_2$ and shows about 150 and 200 mAh g^{-1} of rechargeable capacity when cycled between 2.5 and 4.3 & 2.5 and 4.6 V, respectively. In $LiCo_{1/3}Ni_{1/3}Mn_{1/3}O_2$ the transition metals are in the following oxidation states: Co(III), Ni(II) and Mn(IV). The preparation of an over lithiated material $Li_{1+x}Co_{1/3}Ni_{1/3}Mn_{1/3}O_2$ was shown[9-10] to improve the structure ordering and enhance the cathode cycling and rate capability. In the present paper we are reporting the $LiCo_{1/3}Ni_{1/3}Mn_{1/3}O_2$ compound synthesized through solid state reaction at 900 °C for 18 hours followed by structural characterization, conductivity and dielectric studies at different temperature and frequency by impedance spectroscopy and the magnetic properties through ESR spectroscopy.

Experimental

The cathode compositions were synthesized by a solid-state reaction method from stoichiometric amounts of Li_2CO_3 (Hamada 99.9%), NiO (Hamada 99.9%), Co_2O_3 (Hamada99.9%) and MnO_2 (Hamada 99.9%).

$$0.5Li_2CO_3 + 1/3NiO + 1/3MnO + 1/6Co_2O_3 \rightarrow LiNi_{1/3}Co_{1/3}Mn_{1/3}O_2 + gas \uparrow$$

A slight excess amount of lithium (5%) was used to compensate for any loss of the metal which might have occurred during the calcination at high temperatures. The solid state reaction synthesis method involves three steps. First, the precursors, as raw materials, were well mixed and thoroughly ground with agate mortar, then subjected to heat treatment at a temperature of 500 °C for 5 hours and 800 °C for 10 hours to dry the samples free from gases and impurities. Then, this powder was cooled at the rate of 5 °C/ min. Finally, the mixture was reground and sintered at temperatures 900 °C for 18 hours to complete the chemical reaction in air using a muffle box furnace. The powder samples added with polyvinyl alcohol (PVA) as a binder were ground and then pressed at 5 tons / 6 minutes pressure into a circular disk shaped pellet. The pellet was then sintered at 900 °C for 20 h in air at heating and cooling rates of 5 °C/min. The surface layers of the sintered pellet were carefully polished and washed in acetone and then the pellet was coated with silver paste on the opposite faces which act as electrodes.

The TG/DTG measurement were conducted using Mettler Toledo TG/DTG 851^e instrument from room temperature to 1000 °C in Nitrogen atmosphere at a heating rate of 10 °C /min. The powder x-ray diffraction (XRD) data of the sample was collected on a PANalytical x-pert pro diffractometer with diffraction angles of 10º and 90º in increments of 0.02º. The unit cell lattice parameter was obtained by the unit cell software from the 2θ and (hkl) values. Further, the crystallite size of the sample was obtained by applying the Scherrer's equation from XRD pattern. The particle morphology and elemental analysis of the powders were observed using scanning electron microscopy (SEM) and energy dispersive spectra (EDS) taken from JEOL JSM-6610LV connected with Inca-Penta FETx3.JPG, Oxford Instruments.

Fourier transform infrared (FT-IR) spectra were obtained on a Shimadzu IR-Prestige21 spectrometer using KBr pellet technique in the wave number range between 400 and 1400 cm^{-1}. The electrical measurements were performed using a Phase Sensitive Multimeter (Model: PSM 1700, UK) over the frequency range (50 Hz - 1 MHz) at different temperatures (303.15 K to 393.15 K). Electron spin resonance (ESR) measurements were carried out by using JEOL FA100 instrument at room temperature.

Results and Discussion

Thermal analysis

In order to investigate the possible reactions occurring in the synthesis of $LiNi_{1/3}Co_{1/3}Mn_{1/3}O_2$, thermal analysis was conducted on the precursors. In this work, TG measurements were performed on samples to determine changes in weight in relation to change in temperature. DTG is also done on samples to determine the main phase transition temperatures. All the TG and DTG measurements were carried out in nitrogen atmosphere by heating the powdered samples from room temperature to 1000 °C at a heating and cooling rate of 10 °C /min as shown in Figure 1.

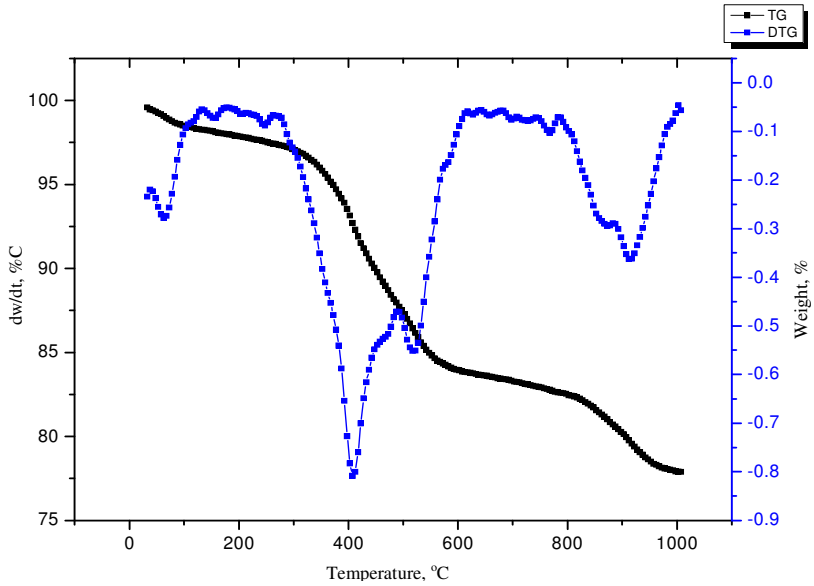

Figure 1. TG/DTG curves for $LiNi_{1/3}Co_{1/3}Mn_{1/3}O_2$

As can be seen from the curves, there is an initial weight loss in the temperature range from room temperature to 310 °C. This corresponds to the evaporation of methanol used during grinding to homogenize the mixture and the moisture absorbed during storage[11]. TG curve of $LiNi_{1/3}Co_{1/3}Mn_{1/3}O_2$ shows significant weight loss (13.8%) between the temperatures 310 °C and 570 °C. This loss is attributed to the decomposition of the precursors Li_2CO_3, NiO_2, CoO_2 and MnO_2 and the reaction between the decomposed materials in order to produce crystalline $LiNi_{1/3}Co_{1/3}Mn_{1/3}O_2$. This is supported by sharp peak observed at 400 °C on the DTG curve. At higher temperatures the TG curve becomes flattened, indicating the stable phase formation. There is little weight loss to be observed over 900 °C, which indicates that the $LiNi_{1/3}Co_{1/3}Mn_{1/3}O_2$ phase has formed at around 900 °C which agrees with proposed synthesis temperature[12,13].

XRD

The x-ray diffraction patterns of $LiNi_{1/3}Co_{1/3}Mn_{1/3}O_2$ calcined at different temperatures are shown in Figure 2. The XRD patterns of the samples are similar to that of $LiCoO_2$ (α-$NaFeO_2$ type, space group $R\bar{3}m$) and can be indexed as hexagonal lattice. The transition metal atoms (M = Ni, Co, Mn) are supposed to be randomly distributed on the 3b sites, whereas the lithium atoms occupy the 3a sites and O atoms occupy the 6c sites. No obvious impurity phase peaks can be observed, indicating that the synthesized samples are single phase at 900 °C for 18 hours. In XRD patterns, the splitting of (006)/(102) peak and (018)/(110) peak are regarded as the indications of characteristic of layered structure materials[14]. From the observation of peak splitting of (006)/(012) and (018)/(110) near 38° and 65°, respectively, it can be seen that the layered structure is well developed[15]. The peak splitting in the XRD pattern of $LiNi_{1/3}Co_{1/3}Mn_{1/3}O_2$ synthesized at 900 °C for 18h shows better property indicating that layered structure is better when the calcination temperature is optimal for the formation of pure phase[16,17]. Figure 3 illustrates the variation of lattice parameter, unit cell volume, intensity ratio and crystallite size with temperature as the values are shown in Table 1.

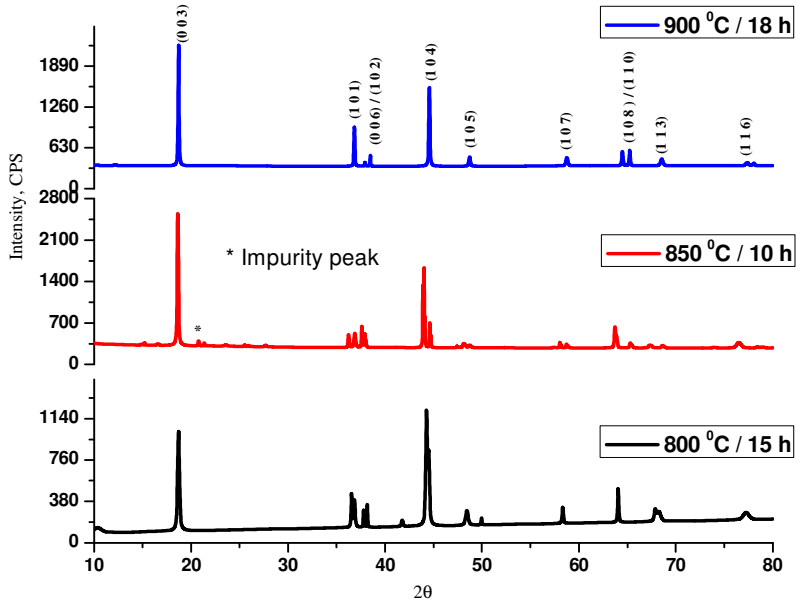

Figure 2. X-ray diffraction patterns of $LiNi_{1/3}Co_{1/3}Mn_{1/3}O_2$ samples synthesized at different temperatures

The crystallographic unit cell parameter values deduced through least squares refinement of these XRD pattern(s) yielded cell parameter values a, c, consistent with the literature reports[18] as listed in Table 1. Also turning to growth of particles crystallites, some insights become possible with estimate of crystallite size made through Debyee Scherrer. Moreover the observed values of $I_{(003)}/I_{(104)}$ for the synthesized compounds is indicated in the Table 1. The value of $(I_{006}+I_{102})/I_{101}$ is called R-factor, which is known to be smaller when the hexagonal ordering is high. The R-value is useful to measure the cation disorder. This value is lowest for the synthesized compound and suggests that the hexagonal ordering is better[19,20].

Table 1. Lattice parameter, unit cell volume, I_{003}/I_{104} and R-factor of $LiNi_{1/3}Co_{1/3}Mn_{1/3}O_2$

Compound	*a* (Å)	c (Å)	V $(Å)^3$	c/*a*	R-factor	I_{003}/I_{104}	Crystallite size nm
850 ºC /20h	2.8761	14.2997	102.4377	4.9719	0.58	0.8388	93.12
900 ºC /10h	2.8518	14.2543	100.3939	4.9984	0.56	1.4175	80.07
900 ºC /18h	2.8899	14.3676	103.9127	4.9717	0.48	1.56	66.69

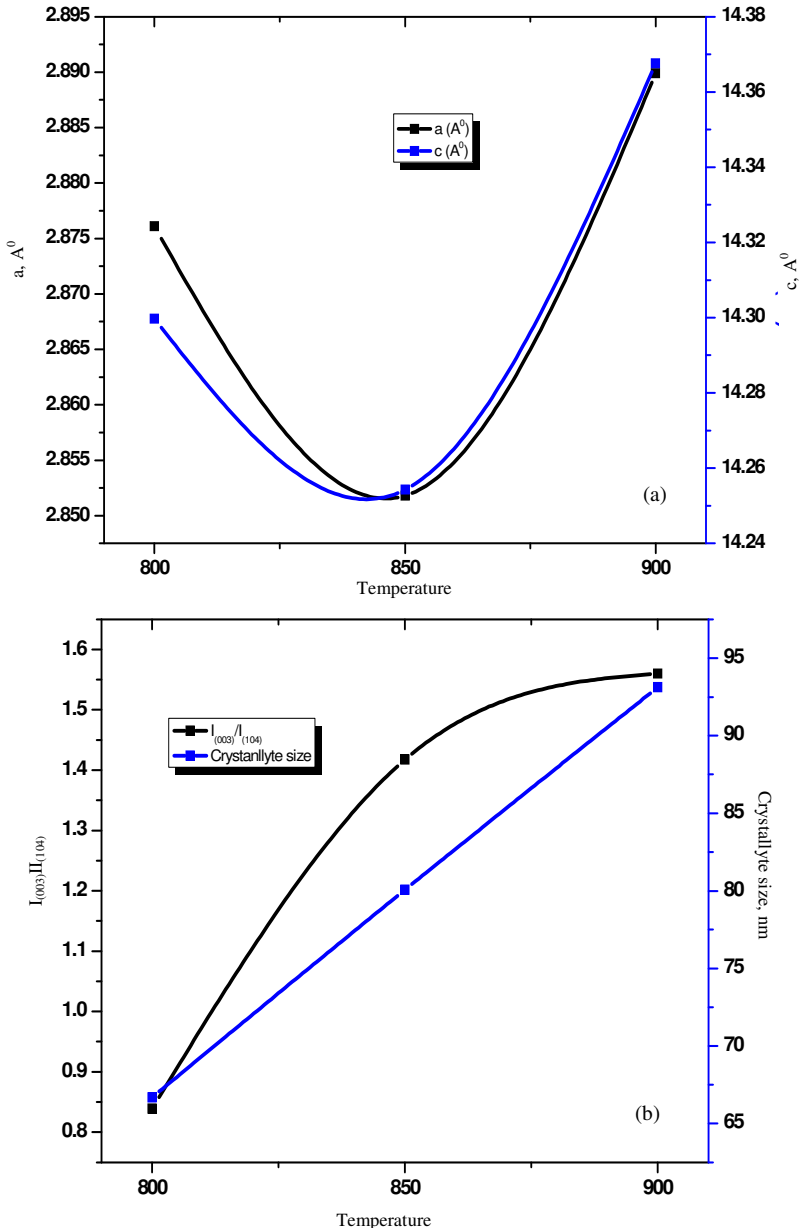

Figure 3. Variation of (a) lattice parameter and (b) crystallite size with temperature

Figure 4(a), show SEM image for $LiNi_{1/3}Co_{1/3}Mn_{1/3}O_2$ sample calcination at temperature, 900 °C for 18h. The primary particles tend to sinter into tight, smooth particles and the particle size rises and reveals well developed primary particles with quite smooth surface and particle size of 0.5-5 µm. Similarly, Figure 4(b) and (c) shows SEM images of $LiNi_{1/3}Co_{1/3}Mn_{1/3}O_2$ samples calcined at 850°C for 10h and 800°C for 15h respectively, reveal the loose, disordered primary particles. From Figure 5 (a), the EDS spectra confirmed the presence of Ni, Co, Mn and O in $LiNi_{1/3}Co_{1/3}Mn_{1/3}O_2$ cathode material. It is clearly observed that the spectra show in Figure 5(b) and (c) the appropriate ratios of the elements. Lithium is not observed in the EDS spectrum because it has too low of an atomic number to be detected with EDS.

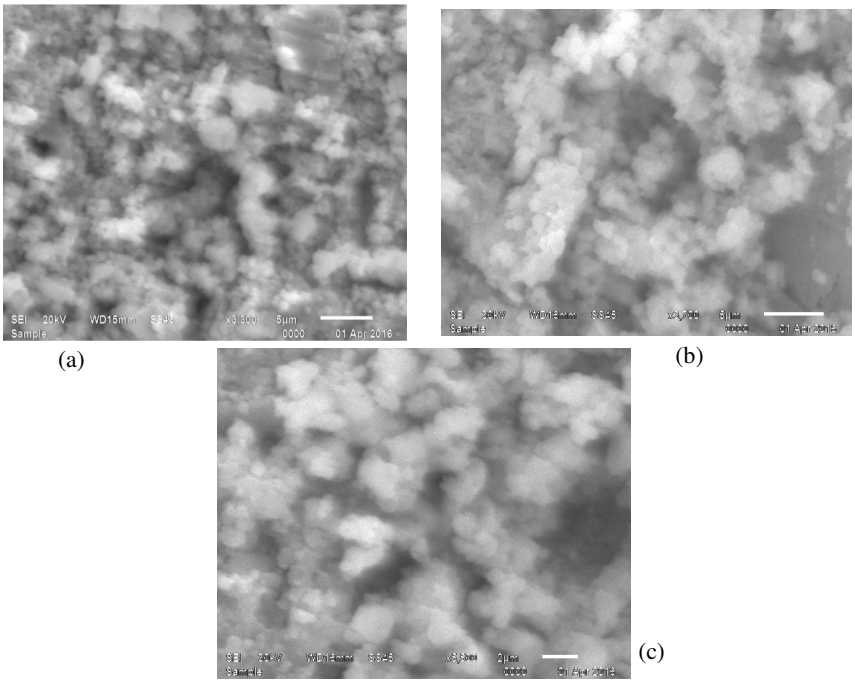

(a) (b) (c)

Figure 4(a-c). SEM images of $LiNi_{1/3}Co_{1/3}Mn_{1/3}O_2$ samples calcined at a temperature (**a**) 900° C/18h, (**b**) 850° C/10h and (**c**) 800° C/15h

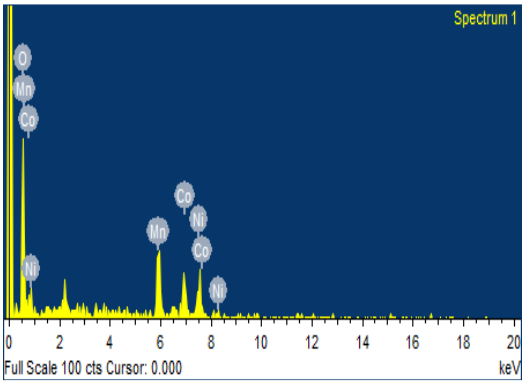

5(a)

Results of Elemental Analysis

Element	Weight %	Atomic %
O	0.60	68.98
Mn	0.38	12.80
Co	0.29	9.21
Ni	0.29	9.01
Total	1.56	

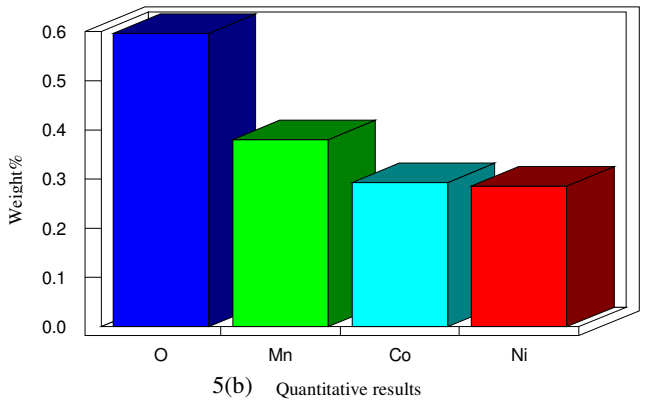

Figure 5. (a) EDS spectra and (b) qualitative results of $LiNi_{1/3}Co_{1/3}Mn_{1/3}O_2$

FTIR

Figure 6 shows FT-IR spectra of the synthesized sample prepared by solid state reaction method calcined at 900 °C for 18 h. In order to validate the results of XRD analysis, the room temperature FT-IR spectra of the synthesized sample was performed. Two distinct peaks are observed in each FT-IR spectrum at different wavelength regions. The two strong frequency bands appeared at wave numbers 623.13 and 521.06 cm^{-1} are responsible for the formation of $LiNi_{1/3}Co_{1/3}Mn_{1/3}O_2$ which might be attributed to asymmetric stretching modes of Li-M-O.

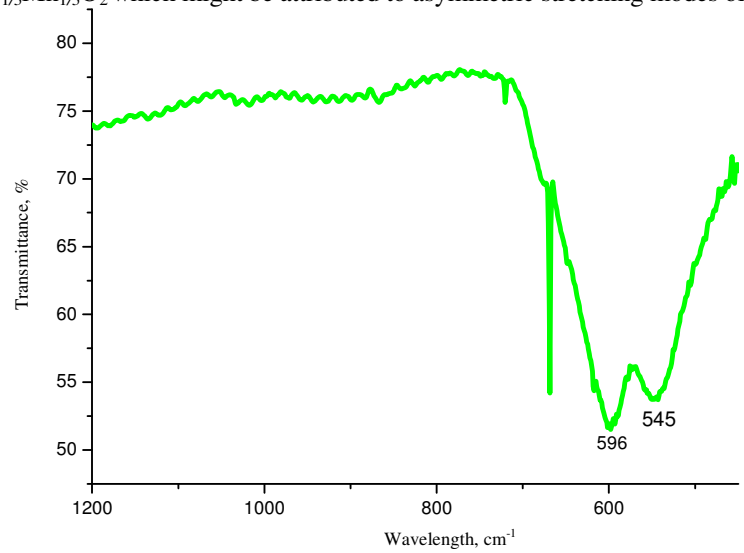

Figure 6. FT-IR spectra of $LiNi_{1/3}Co_{1/3}Mn_{1/3}O_2$ sample calcined at a temperature 900 °C/18 h

Impedance analysis

Electrochemical impedance spectroscopy (EIS) is a powerful tool to identify the kinetics of lithium intercalation/deintercalation into electrodes. In general, electrochemical impedance studies were carried out to have better understanding of certain aspects of a lithium cell such as failure mechanism[21], self discharge[22], lithium cycling efficiency[23], interfacial phenomenon between electrode and electrolyte[24] and lithium cation diffusion in the and

electrode and the electrolyte[25]. Moreover, the EIS measurement technique is also useful to investigate the temperature and frequency dependent behaviour of ac conductivity and dielectric constant. The obtained results from these analyses can provide information about the electrical behaviour of the samples. Moreover the ac technique has been developed to measure impedance over a range of frequencies to estimate the exact bulk conductivity and frequency dependant. From the impedance study, one can obtain not only the bulk conductivity but also grain boundary effects, ionic transport, double layer formation at the electrode/electrolyte interface. In the present study, the electrical properties of $LiNi_{1/3}Co_{1/3}Mn_{1/3}O_2$ compound taken at wide frequency range (50 Hz - 1MHz) at different temperatures (303.15 K to 393.15 K).

Cole-Cole

Figure 7 shows the AC Impedance plots of $LiNi_{1/3}Co_{1/3}Mn_{1/3}O_2$ taken wide frequency range (50 Hz-1 MHz) at different temperatures (303.15 K to 393.15 K). Semicircles were observed on the real axis at the high frequency range. In the low frequency range, nearly straight line with a certain angle to the real axis corresponds to the Warburg impedance. The high frequency semicircle is related to the charge-transfer resistance and the double-layer capacitance. The low frequency tails resulted from the diffusion of lithium ions in the bulk active mass. In the case of $LiNi_{1/3}Co_{1/3}Mn_{1/3}O_2$ the diameter of the semicircle significantly depends on the potential during charging, indicating that the film formation process is dependent on the lithium ion content. On the other hand, the charge transfer resistance shows a greater dependence on the lithium insertion and extraction levels.

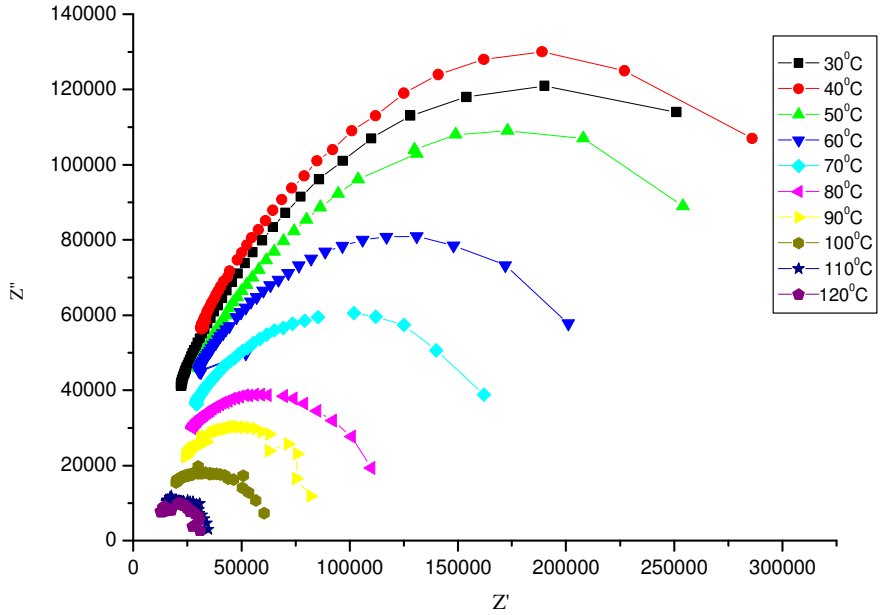

Figure 7. Cole-Cole plots for $LiNi_{1/3}Co_{1/3}Mn_{1/3}O_2$ sample calcined at a temperature 900 °C/18 h

AC conductivity

The frequency dependence of the conductivity for $LiNi_{1/3}Co_{1/3}Mn_{1/3}O_2$ wide frequency range (50 Hz-1 MHz) at different temperatures (303.15 K to 393.15 K) shown in the Figure 8. A typical frequency dependence conductivity spectrum exhibit three distinguished regime:

a) low frequency dispersed b) an intermediate plateau and c) Conductivity dispersion at high frequency. The variation of conductivity in low frequency region may be attributed to the polarization effects at the electrode interface. At very low frequencies, more charge accumulation occurs and hence, drop in conductivity. In the intermediate frequency region, conductivity is almost found to be frequency independent and equal to dc conductivity and at the high frequency region, the conductivity increases with frequency. The variations of ac conductivity with temperature are shown in Table 2. The activation energy is obtained from Arrhenius relation and it is found to be 0.3422 eV. Generally, ion diffusion pathways and activation energies that govern Li-ion transport within cathode materials are of considerable interest when considering rates at which a battery can be charged and discharged. In this work, the low activation energy suggests that this compound is a good conductor and suitable to cathode materiel for lithium ion battery.

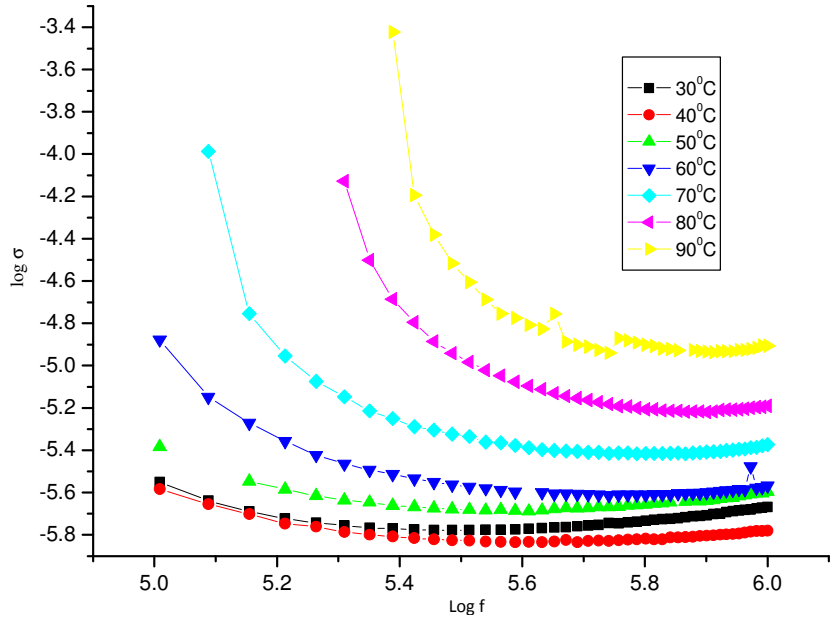

Figure 8. Variation of Conductivity with frequency for $LiNi_{1/3}Co_{1/3}Mn_{1/3}O_2$ sample calcined at a temperature 900 °C/18 h

Table 2. Variation of ac conductivity with temperature at 1 MHz

Temperature, °C	ac conductivity, S/cm
30	$2.15x10^{-6}$
40	$1.66x10^{-6}$
50	$2.53x10^{-6}$
60	$2.71x10^{-6}$
70	$4.23x10^{-6}$
80	$6.45x10^{-6}$
90	$1.24x10^{-5}$
100	$3.14x10^{-5}$
110	$1.73x10^{-4}$
120	$1.01x10^{-2}$

Dielectric constant (ε')

The variation of the dielectric constant (ε') as function of frequency range (50 Hz - 1 MHz) at different temperatures (303.15 K to 393.15 K) for $LiNi_{1/3}Co_{1/3}Mn_{1/3}O_2$ samples is shown in Figure 9. From the frequency dependent plot of ε', it is observed that the value of ε' decreases sharply as the frequency increases and attains a constant limiting value, at which ε' becomes almost frequency independent. The higher values of dielectric constant at low frequencies can be due to pile-up of charges at the interfaces between the sample and the electrode. This can be explained based on the behaviour of the dipole movement as follows. Dielectric behaviour of samples with frequency is related to the applied electric field. An alternating electric field changes its direction with time. With each direction reversal, the polarization components are required to follow the field reversal. So, the polarization depends on the ability of dipoles to orient themselves in the direction of the field during each alternative change of the field. At low frequency regions the dipoles will get sufficient time to orient themselves completely along the direction of the field, resulting in larger values of ε' of the samples. As the frequency increases further, the dipoles in the sample cannot reorient themselves fast enough to respond to the applied electric field, resulting in the decrease in ε' of the samples and becoming almost constant.

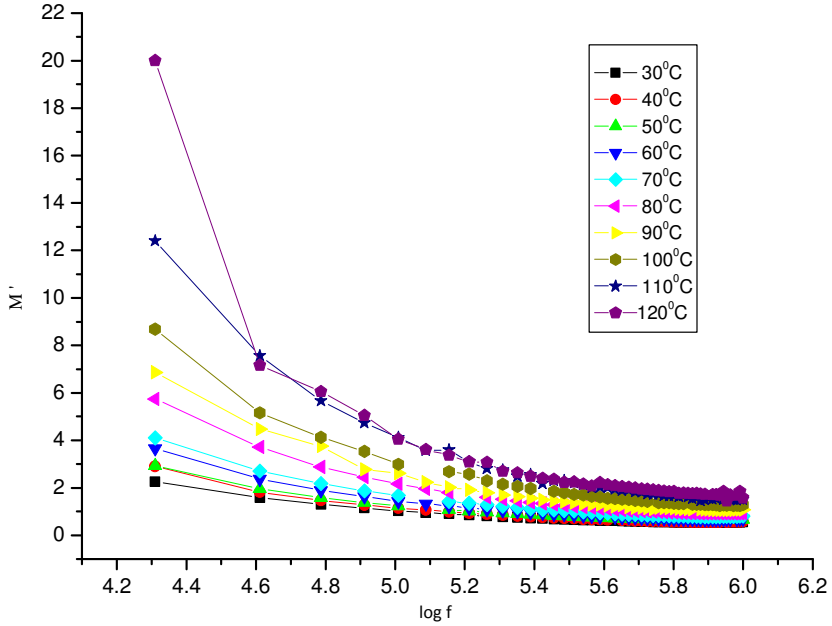

Figure 9. Variation of the dielectric with frequency for $LiNi_{1/3}Co_{1/3}Mn_{1/3}O_2$ sample calcined at a temperature 900° C/18 h

Dielectric loss (tanδ)

The dielectric loss (*tanδ*) that was ascribed to conduction most probably involves the migration of ions over longer distances. This motion is the same as that occurring under direct current conductions. The variation of the dielectric loss *tanδ* with frequency range (50 Hz-1 MHz) at different temperatures (303.15 K to 393.15 K) shown in Figure 10 for $LiNi_{1/3}Co_{1/3}Mn_{1/3}O_2$. The magnitude of the dielectric loss increases with increase in frequency. At low frequency conduction losses have minimum value. As the frequency

increases ac conductivity is also increases, so the conduction losses increase. This leads to increase of the value of *tanδ* with frequency. The increase of the dielectric loss at low frequency is due to dipole polarization.

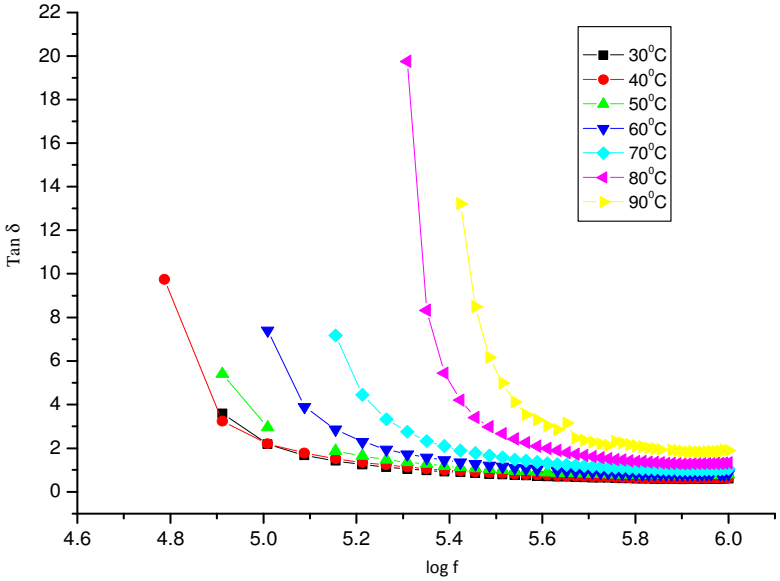

Figure 10. Variation of the dielectric loss tanδ with the frequency for $LiNi_{1/3}Co_{1/3}Mn_{1/3}O_2$ sample calcined at a temperature 900 °C/18 h

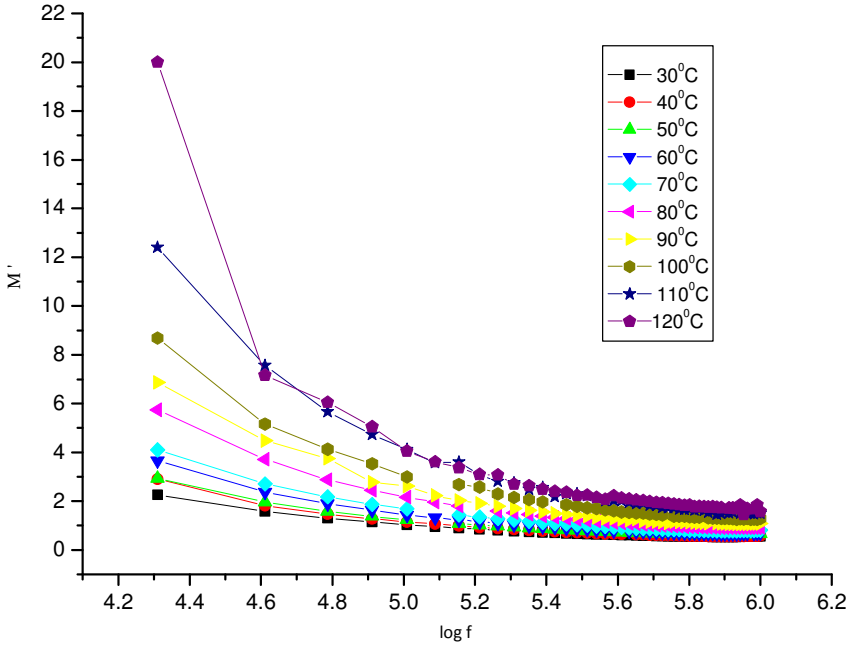

Figure 11. The variation of electric modulus with frequency for $LiNi_{1/3}Co_{1/3}Mn_{1/3}O_2$ sample calcined at a temperature 900 °C/18 h

Electric modulus

The complex electric modulus spectra represent the measure of the distribution of ion energies or configurations in the structure and also describe the electrical relaxation of ion conducting lattices as a microscopic property of materials[26-28]. The real (M') and imaginary (M") parts of electric modulus (M*) were calculated using the real and imaginary parts of impedance data measured at different frequencies for $LiNi_{1/3}Co_{1/3}Mn_{1/3}O_2$ sample and pellet dimensions. The variation of the electric modulus as function of frequency with frequency range (50Hz-1MHz) at different temperatures (303.15 K to 393.15 K) for $LiNi_{1/3}Co_{1/3}Mn_{1/3}O_2$ samples is shown in Figure 11. The first one in the low frequency region the electric modulus decreases with frequency and almost frequency independent in the intermediate regions.

ESR

Figure 12 shows the ESR spectra of $LiNi_{1/3}Co_{1/3}Mn_{1/3}O_2$ cathode material measured at room temperature. The ESR spectrum of $LiNi_{1/3}Co_{1/3}Mn_{1/3}O_2$ consists of a very broad signal centred at about H_0= 336 mT. The position of the centre of the signal is close to the value expected for uncorrelated spins with the gyromagnetic factor g = 2.01. g is proportionality factor, function of electron's environment, also called as spectroscopic splitting factor or Lande's splitting factor.

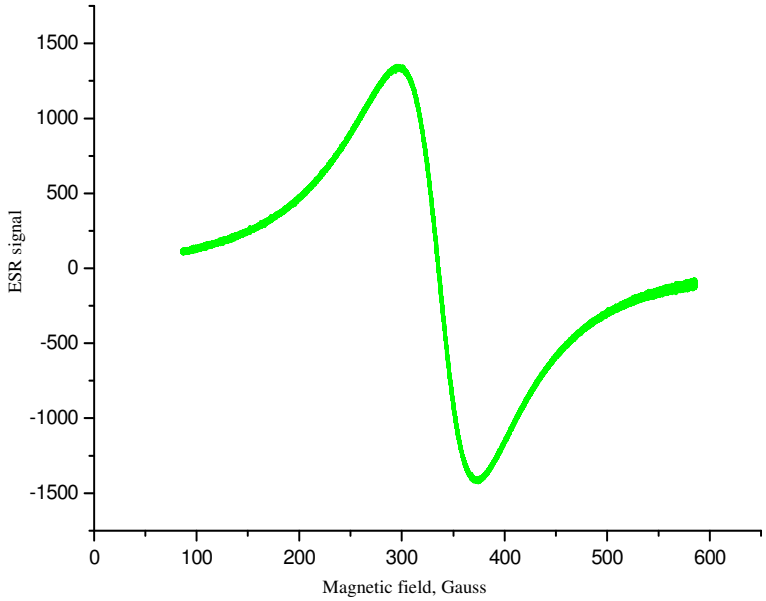

Figure 12. ESR spectra for $LiNi_{1/3}Co_{1/3}Mn_{1/3}O_2$ sample calcined at a temperature 900 °C/18h

Conclusion

Layered structure $LiNi_{1/3}Co_{1/3}Mn_{1/3}O_2$ was synthesized by solid state reaction method and Structural, morphological, magnetic and impedance studies of $LiNi_{1/3}Co_{1/3}Mn_{1/3}O_2$ cathode was investigated. In order to investigate the possible reactions occurring in the synthesis of $LiNi_{1/3}Co_{1/3}Mn_{1/3}O_2$, TG/DTG analysis is conducted on the precursor in N_2 atmosphere. From x-ray diffraction analysis the compound possesses a typical α-$NaFeO_2$ layered

structure with $R\bar{3}m$ space group. The SEM morphology shows a very fine surface morphology and the crystal grains. The EDS spectra confirmed the presence of Ni, Co, Mn and O in $LiNi_{1/3}Co_{1/3}Mn_{1/3}O_2$ cathode material. Two distinct peaks are observed in each FT-IR spectrum at different wavelength regions. The two strong frequency bands appeared at wave numbers 623.13 and 521.06 cm^{-1} are responsible for the formation of $LiNi_{1/3}Co_{1/3}Mn_{1/3}O_2$ which might be attributed to asymmetric stretching modes of Li-M-O. The impedance, dielectric, Dielectric loss (tanδ) and modulus studies of $LiNi_{1/3}Co_{1/3}Mn_{1/3}O_2$ is carried out as function of frequency with frequency range (50 Hz - 1 MHz) at different temperatures (303.15 K to 393.15 K) for $LiNi_{1/3}Co_{1/3}Mn_{1/3}O_2$ samples and the results are presented. From ESR analysis of magnetic measurements, the presence of unpaired spins was estimated. From this study, we conclude that the layered $LiNi_{1/3}Co_{1/3}Mn_{1/3}O_2$ material is prepared by solid-state reaction method at 900 °C for 18 h is promising next-generation cathode material for lithium ion batteries.

References

1. Yin S C, Rho Y H, Swainson I and Nazar L F, *Chem Mater.*, 2006, **18**, 1901-1910; DOI:10.1021/cm0511769
2. Roberts M and Owen J, *ACS Comb Sci.*, 2011, **13(2)**, 126-134; DOI:10.1021/co100028m
3. Yabuuchi N and Ohzuku T, *J Power Sources*, 2003, **119-121**, 171-174; DOI:10.1016/S0378-7753(03)00173-3
4. Chen Y, Wang G X, Konstantinov K, Liu H K and Dou S X, *J Power Sources,* 2003, **119-121**, 184-188; DOI:10.1016/S0378-7753(03)00176-9
5. Zhecheva E and Stoyanova R, *Solid State Ionics*, 1993, **66(1-2)**, 143-149; DOI:10.1016/0167-2738(93)90037-4
6. Stewart S G, Srinivasan V and Newman J, *J Electrochem Soc.*, 2008, **155**, A664-A671; DOI:10.1149/1.2953524
7. Martha S K, Sclar H, Framowitz Z S, Kovacheva D, Saliyski N, Gofer Y, Sharon P, Golik E, Markovsky B and Aurbach D, *J Power Sources*, 2009, **189(1)**, 248-255; DOI:10.1016/j.jpowsour.2008.09.090
8. Ohzuku T, Nakura K and Aoki T, *Electrochim. Acta*, 1999, **45(1-2)**, 151-160; DOI:10.1016/S0013-4686(99)00200-5
9. Kobayashi H, Arachi Y, Emura S, Kageyama H, Tatsumi K and Kamiyama T, *J Power Sources*, 2005, **146(1-2)**, 640-644; DOI:10.1016/j.jpowsour.2005.03.081
10. Park S H, Kang S H, Belharouak I, Sun Y K and Amine K, *J Power Sources*, 2008, **177(1)**, 177-183; DOI:10.1016/j.jpowsour.2007.10.062
11. Jouanneau S and Dahn J R, *Chem Mater.*, 2003, **15(2)**, 495-499; DOI:10.1021/cm020818e
12. Caballero A, Cruz M, Hernan L and Melero M, *J Power Sources*, 2005, **150**, 192-201; DOI:10.1016/j.jpowsour.2005.02.013
13. Ben K, Amdouni N, Abdel-Ghany A, Zaghib K, Mauger A, Gendron F and Julian C M, Ionics, 2008, 14, 89-97.
14. Xiaoyu Z, Mauger A, Lu Q, Groult H, Perrigaud L, Gendron F and Julian C M, *Electrochim Acta*, 2010, **55(22)**, 6440-6449; DOI:10.1016/j.electacta.2010.06.040
15. Youngsik K, Hyun S K and Steve W M, *Electrochim Acta*, 2006, **52,** 1316-1322; DOI:10.1016/j.electacta.2006.07.033
16. Dahn J R, Von Sacken U and Michal C A, *Solid State Ionics*, 1990, **44(1-2)**, 87-97; DOI:10.1016/0167-2738(90)90049-W

17. Sung-Keun K, Woon-Tae J, Hong-Ki L and Joongpyo S, *Int J Electrochem Sci*., 2008, **3**, 1504-1511.
18. Peng Y, Zhixing W, Wenjie P, Lingjun L, Wei C, Huajun G and Xinhai L,. *Powder Technology*, 2011, **214(3)**, 279-282; DOI:10.1016/j.powtec.2011.08.022
19. D'Epifanio A, Croce F, Ronci F, Rossi V A, Traversa E and Scrosati B, *Chem Mater*., 2004, **16(18)**, 3559-3564; DOI:10.1021/cm040130x
20. Qinglai J, Ke D and Yuehui H, *Electrochim Acta*, 2013, **107**, 133-138; DOI:10.1016/j.electacta.2013.05.148
21. Periasamy P, Kalaiselvi N and Kim H S, *Int J Electrochem Sci*., 2007, **2**, 689-699.
22. Pistoia G, Antonin A, Rosati R and Zane D, *Electrochim Act*, 1996, **41(17)**, 2683-2689; DOI:10.1016/0013-4686(96)00122-3
23. Montesperelli G, Nunziante P, Pasquili M and Pistoia G, *Solid State Ionics*, 1990, **37(2-3)**, 149-156; DOI:10.1016/0167-2738(90)90238-M
24. Gaberscek M and Pejovnik S, *Electrochim Acta,* 1996, **41**, 1137-1142; DOI:10.1016/0013-4686(95)00464-5
25. Dillip K Pradhan R N, Choudhary P and Samantaray B K, *Express Polym Lett.,* 2008, **2(9)**, 630-638; DOI:10.3144/expresspolymlett.2008.76
26. Macedo P B, Moynihan C T and Bose R, *Phys Chem Glasses*, 1972, **13,** 171-179.
27. Provenzano V, Boesch L P, Volterra V, Moynihan C T and Macedo P B, *J Am Ceram Soc*, 1972, **55**, 492-496.
28. Muralidharan P, Nallamuthu N, Prakash I, Satyanarayana N and Venkateswarlu M, *J Am Ceram Soc.*, 2007, **90(1)**, 125-131; DOI:10.1111/j.1551-2916.2006.01355.x